UMT PRESS

Journal of Sustainability Science and Management
Journal Homepage: https://jssm.umt.edu.my
eISSN: 2672-7226
DOI: http://doi.org/10.46754/jssm.2026.01.008

SOLVOTHERMAL SYNTHESIS-DRIVEN NANOSIZED $CoFe_2O_4$ ANODE AND THE ELECTROCHEMICAL STUDIES FOR SODIUM STORAGE

SARAH UMEERA MUHAMAD[1], NURUL HAYATI IDRIS[1]*, HANIS MOHD YUSOFF[2], SITI ROHANA MAJID[3], MUHAMAD FAIZ MD DIN[4] AND LUKMAN NOEROCHIM[5]

[1]Energy Storage Research Group, Faculty of Ocean Engineering Technology, Universiti Malaysia Terengganu, 21030 Kuala Nerus, Terengganu, Malaysia. [2]Advanced Nano Material Research Group, Faculty of Science and Marine Environment, Universiti Malaysia Terengganu, 21030 Kuala Nerus, Terengganu, Malaysia. [3]Centre for Ionics University of Malaya, Department of Physics, Faculty of Science, University of Malaya, 50603 Kuala Lumpur, Malaysia. [4]Department of Electrical and Electronic Engineering, Faculty of Engineering, National Defence University of Malaysia, Kem Sungai Besi, 57000 Kuala Lumpur, Malaysia. [5]Department of Materials and Metallurgical Engineering, Institut Teknologi Sepuluh Nopember, Surabaya, 60111 Indonesia.

**Corresponding author: nurulhayati@umt.edu.my*

ARTICLE INFO

Article History:
Received: 21 October 2024
Revised: 30 May 2025
Accepted: 7 July 2025
Published: 15 January 2026

Keywords:
Sodium-ion batteries, anode, $CoFe_2O_4$, solvothermal, electrochemical performances.

ABSTRACT

Spinel ferrites have been widely explored as an alternative negative electrode in sodium-ion (Na-ion) batteries because of their high theoretical capacity arising from the synergistic effect of two metal ions and better electronic conductivity compared with single-metal oxides. In this work, $CoFe_2O_4$ nanoparticles were successfully prepared using the solvothermal technique, followed by calcination at 700°C and 800°C. The influences of the calcination temperature and time on the structural, morphological, and battery performances of $CoFe_2O_4$ were investigated. $CoFe_2O_4$ calcined at 700°C for 2 hours revealed small particles with a well-defined crystallinity, as confirmed by electron microscopy. When tested as an anode for Na-ion batteries, the $CoFe_2O_4$ electrode delivered a high reversible discharge capacity (352 mAh g^{-1} at 0.1 C rate) and a reasonable cyclability (97 mAh g^{-1} up to 100 cycles) and reached ~99% Coulombic efficiency. The results showed that the small particle size, porous structure and well-defined crystal structure of $CoFe_2O_4$ improved the battery performances by providing a shorter, more effective diffusion channel for the Na^+ ions and hindered the pulverisation during the charge or discharge process.

Introduction

Renewable energy resources are being investigated as potential alternatives to fossil fuels for future energy storage systems such as supercapacitors and rechargeable batteries (Scrosati *et al*., 2011; Yan *et al*., 2018). In this situation, sodium-ion (Na-ion) batteries have gained increasing interest because of their natural abundance in the Earth's crust and affordability, thereby offering a potential replacement for lithium-ion (Li-ion) batteries. However, Na-ion has 55% larger ionic radius than Li-ion, and most materials lack sufficiently large interstitial spaces within their crystallographic structures to accommodate Na-ions (Cao *et al*., 2012).

The development of viable anode materials remains as a critical challenge for achieving future high-performance Na-ion batteries. On the anode side, most studies have focused on transition metal oxides (TMOs), which are attractive because of their high specific capacity, low cost, and enhanced safety (Wang *et al*., 2018). However, the most common problems with TMOs are their large volume expansion and contraction (swelling and shrinking of active materials) during sodiation and desodiation,

which promote capacity fading (Jian *et al*., 2014; Hwang *et al*., 2017). Hariharan *et al*. (2013) examined the sodiation and desodiation characteristics of the Fe_3O_4 electrode, which was capable of delivering an initial discharge capacity of 643 mAh g^{-1}. However, the material exhibited a very poor capacity retention with nearly 50% irreversibility.

Volvo *et al*. (2014) produced nanostructured Fe_2O_3 for Na-ion with a specific capacity of 250 mAh g^{-1} at 130 mA g^{-1} after 60 cycles. Despite these encouraging advancements, the identification of Fe-based oxide materials with acceptable specific capacity and cyclability for Na-ion batteries remains as a significant challenge.

Spinel ferrites (MFe_2O_4; M = Mn, Mo, Co, Cu, and Ni) have gained significant interest as favourable anode materials for Na-ion batteries. They offer numerous benefits, including inexpensive cost, remarkable synergetic effect, high Na storage, and excellent conductivity (Yuan *et al*., 2014; Cao *et al*., 2017; He *et al*., 2017). Cobalt ferrite ($CoFe_2O_4$) is particularly interesting because of its high theoretical capacity of 916 mAh g^{-1}. Several approaches are being used to synthesise $CoFe_2O_4$, including ball milling (Dehghanpour, 2016), mechanical alloying (Ding *et al*., 1995), molten salt (Muhamad *et al*., 2023), and hydrothermal (Li *et al*., 2010).

Among these approaches, solvothermal techniques have become notably favoured and widely adopted because of their cost-effectiveness and scalability for large-scale production. This technique is notably effective in producing highly crystalline nanomaterials with uniform size and shape, high purity, and well-controlled morphology (Jiang *et al*., 2024). Duang *et al*. (2021) used the solvothermal method to synthesise $CoFe_2O_4$ using cobalt nitrate and iron nitrate as precursors, with the addition of oleic acid as a surfactant. They obtained $CoFe_2O_4$ nanoparticles with particles sizes ranging between 5.5 and 12.0 nm.

Creating nanoparticles is a promising technique for enhancing the rate capability performances of Na-ion batteries because it increases the surface area, reduces the diffusion length and accelerates the sodiation and desodiation rates of Na-ions. The synthesis methods can significantly influence the morphologies, structure, phase purity, and crystallinity of $CoFe_2O_4$ (Safi *et al*., 2016). $CoFe_2O_4$ with various morphologies and structures are investigated as the high-performance anode in Na-ion batteries.

Zhang *et al*. (2017) developed a porous $CoFe_2O_4$ nanocube by annealing the metal-organic framework Prussian blue as a precursor. This porous $CoFe_2O_4$ nanocube exhibited a specific capacity of 360 mAh g^{-1} at 50 mA g^{-1} after 50 cycles. Additionally, Zhou *et al*. (2019) produced hollow $CoFe_2O_4$ using a spherical CoFe-glycerate self-template hydrothermal technique. The resulting hollow $CoFe_2O_4$ electrodes showed good cyclability (~100 mAh g^{-1} after 100 cycles at 50 mA g^{-1}). In another report, He *et al*. (2017) synthesised $CoFe_2O_4$ using the hydrothermal method and achieved the first discharge capacity of 300 mAh g^{-1} at 100 mA g^{-1}.

Similarly, Feng *et al*. (2017) synthesised $CoFe_2O_4$ using the hydrothermal technique and showed noteworthy electrochemical properties. After 90 cycles, the $CoFe_2O_4$ possessed a discharge capacity of 200 mAh g^{-1} at 0.05 mA g^{-1}. Although nanoparticle development could possibly improve the rate capability performance, the electrochemical stability also critically relied on the precise conditions of the synthesis process, requiring further investigation into the optimisation of these parameters for improved Na-ion batteries.

To the best of our knowledge, there has been limited research on the morphology, phase purity and particle size of $CoFe_2O_4$ nanoparticles determined by a solvothermal technique that does not involve surfactants, carbon coatings, or templates. The solvothermal method provides numerous benefits, including the ability to produce nanomaterials at a low reaction temperature and a high pressure, as well as the high particle uniformity. Herein, a

straightforward approach for producing bulk material through the solvothermal method with ethanol as the solvent is reported. Ethanol plays a crucial role in controlling the nucleation and growth of $CoFe_2O_4$ nanoparticles, resulting in smaller, more uniformly sized particles (Repko *et al*., 2011).

In fact, smaller particles significantly enhance the contact area between the electrode and the electrolyte, improving the intercalation and deintercalation of Na-ions and ultimately leading to a higher discharge capacity. Consequently, the Na storage performance of the $CoFe_2O_4$ electrodes was greatly improved. At 0.1 C rate, the $CoFe_2O_4$ electrode exhibited a reversible discharge capacity of 352 mAh g^{-1} (at the second cycle). After 100 cycles, $CoFe_2O_4$ slowly decreased to 97 mAh g^{-1} with ~99% Coulombic efficiency.

The enhanced cyclability and rate capability of $CoFe_2O_4$ synthesised through the solvothermal method in this study may provide valuable insights for the future research on its potential application in Na-ion batteries.

Materials and Methods

Synthesis of Spinel $CoFe_2O_4$

The $CoFe_2O_4$ nanoparticles were prepared using the solvothermal method following this procedure: The initial precursors containing cobalt (II) chloride hexahydrate ($CoCl_2 \cdot 6H_2O$, ≥ 99.0; Sigma-Aldrich) and iron chloride ($FeCl_3$, ≥ 98%; Sigma-Aldrich) were dissolved in 60 mL ethanol and stirred for 1 hour (h). Next, hydrazine hydrate was added and stirred vigorously for another 10 minutes before being transferred to a 125 mL Teflon-lined, stainless-steel autoclave. The sealed autoclave reactor was placed in an oven and heated at 150°C for 12 hours.

Subsequently, the precipitate was separated by centrifugation several times with deionised water, followed by drying at 60°C overnight under vacuum. Finally, the $CoFe_2O_4$ powders were obtained by calcinating the precursors at 700°C and 800°C for 2 and 6 hours, respectively. The powders were denoted as 700°C 2 h, 700°C 6 h, 800°C 2 h, and 800°C 6 h.

Material Characterisation

The structural morphologies of $CoFe_2O_4$ was characterised using several techniques: X-ray diffraction (XRD) with Rigaku MiniFlex II, nitrogen (N_2) adsorption–desorption isotherms with Micromeritics ASAP 2020 System, scanning electron microscopy (SEM) with JEOL JSM-6360LA, transmission electron microscopy (TEM) with TECNAI G2 F20, Fourier-transform infrared (FTIR) spectroscopy with Shimadzu IR Tracer-100, X-ray photoelectron spectroscopy (XPS) with Axis-Ultra DLD XPS Kratos, and Raman spectroscopy with Renishaw System using 532 nm radiation at 0.1% laser power.

Electrochemical Measurements

For electrochemical characterisation, the electrode consists of 75 wt.% $CoFe_2O_4$, 15 wt.% carbon black (> 99.5%, Sigma-Aldrich), and 10 wt.% polyvinylidene fluoride (PVDF) (Sigma-Aldrich). The mixture was dissolved in N-methyl-2-pyrrolidone (NMP) (≥ 99.0, Sigma-Aldrich) and ground to ensure homogeneity.

The slurry was pasted onto a piece of copper foil and dried at 100°C for 24 hours under vacuum. The active material load for each electrode was approximately 2 mg cm^{-2}. The separator used was glass fibre (GF/D). The counter electrode used was sodium metal (99.9% trace metal basis, Sigma-Aldrich). The electrolyte was prepared by dissolving 1 M $NaClO_4$ (98%, Sigma-Aldrich) in anhydrous propylene carbonate (anhydrous, 99.7%, Sigma-Aldrich), added with 5 wt.% fluoroethylene carbonate (99%, Sigma-Aldrich).

To fabricate a coin cell (CR2032), all electrodes were assembled in a glovebox (MBRAUN, Unilab, Germany). The electrochemical characteristics of the $CoFe_2O_4$ electrode was investigated in the voltage range of 0.01 to 3.00 V. Specifically, the galvanostatic charge–discharge was performed at various current rates (1 C = 916 mA g^{-1})

using a NEWARE battery testing system. Cyclic voltammetry was conducted using CHI 700E at a scan rate of 0.1 mV s^{-1}.

Results and Discussions

Figure 1 depicts a schematic diagram of the synthesised $CoFe_2O_4$ via the solvothermal method at 150°C for 12 hours, followed by air calcination. The solvothermal method is effective in obtaining nanoparticles less than 100 nm in size. During the solvothermal synthesis involving $CoCl_2 \cdot 6H_2O$ and $FeCl_3$ in ethanol, significant reactions include nucleation, followed by growth into intermediate cobalt ferrite nanoparticles. Ethanol not only acts as a reaction medium but also serves as a dissolver to form solvent–reactant complex, thereby influencing the chemical reaction rate. The present hydrazine hydrate as a reduction agent also accelerates the reduction kinetics of metal salts (Rafienia *et al*., 2018). The possible reaction occurring during the synthesis can be ascribed to the following:

$$CoCl_2 \cdot 6H_2O + 2FeCl_3 \rightarrow CoFe_2O_4 + 2H_2O + 8HCl + CO_2 \quad (1)$$

The crystallographic structure of $CoFe_2O_4$ was determined using XRD and subsequently refined using the Rietveld refinement technique (Figure 2). $CoFe_2O_4$ powder was obtained through calcination at the following conditions: (a) 700°C 2 h, (b) 800°C 2 h, (c) 700°C 6 h, and (d) 800°C 6 h. The spinel structure of $CoFe_2O_4$ was consistent with all of the diffraction peaks' characteristics (JCPDS No. 22-1086) and no intermediate phase was observed. Evidently, the XRD peak intensity and the precision of well-defined peaks both increased as the calcination temperature increased, suggesting that the crystallinity improved as a result of crystal growth and the minimisation of the interfacial surface energy (Kumar *et al*., 2013; Ranjith Kumar *et al*., 2014; Gao *et al*., 2018).

This also suggests that the solvothermal technique can be employed to rapidly and cost-effectively synthesise highly pure $CoFe_2O_4$ particles with a spinel crystalline phase. The average particle sizes were calculated as follows using the Debye–Scherrer equation to obtain the average crystallite size (L) according to Equation (2):

$$L = \frac{k\lambda}{\beta \cos \theta} \quad (2)$$

Here, k is a constant (0.9394); λ is the Cu–Kα radiation wavelength (1.5148 Å); β is the full width at half maximum of the XRD peak (in radian); and, θ is the diffraction angle. The average particle size was calculated using the most intense peak. L increased with the increasing temperature, ranging from 27.69 to 32.66 nm. As presented in Table 1, the $CoFe_2O_4$ nanoparticles possessed lattice parameters ranging between 8.3726 and 8.3718 Å, consistent with those in a previous report (Prabhakaran *et al*., 2017). The slight reduction in the lattice parameters may

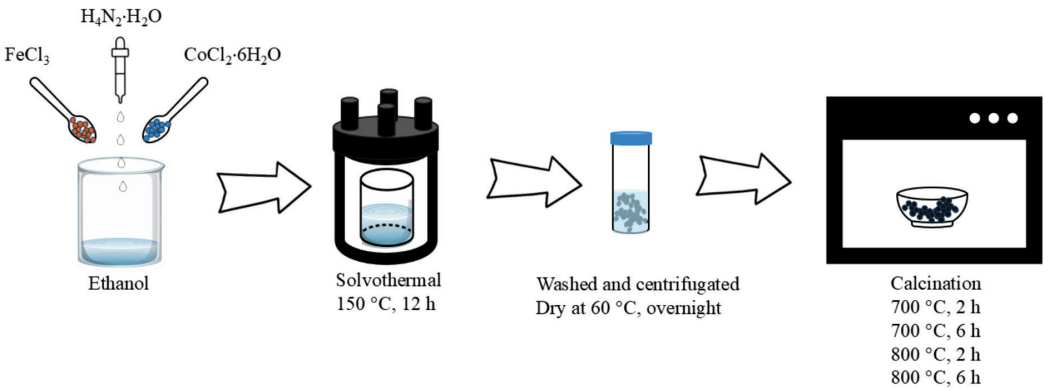

Figure 1: Schematic illustration of the preparation process of the $CoFe_2O_4$ using solvothermal

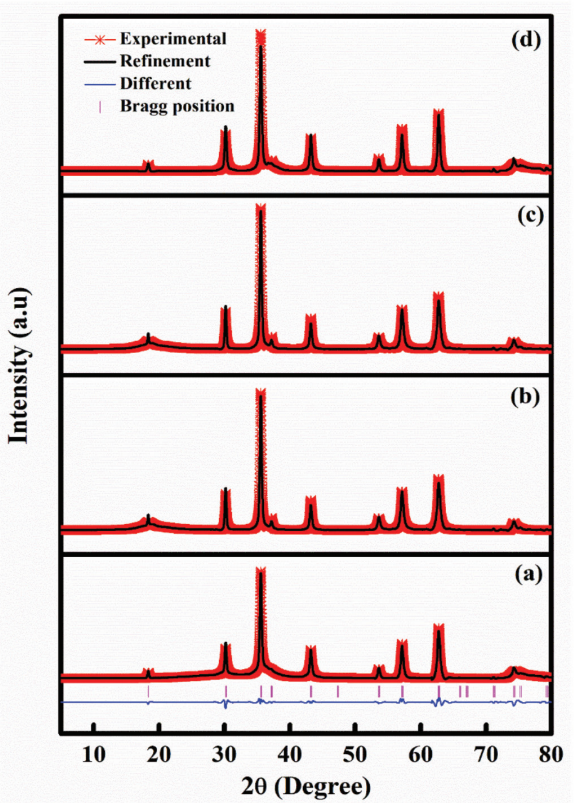

Figure 2: Rietveld refinements result of the XRD data for sample (a) 700°C 2 h, (b) 800°C 2 h, (c) 700°C 6 h, and (d) 800°C 6 h

Table 1: Rietveld refinements result for sample 700°C 2 h, 800°C 2 h, 700°C 6 h, and 800°C 6 h

Sample	*a* (Å)	*c* (Å)	Bragg R_{factor} (%)	$R_{f\ factor}$ (%)	x^2
700°C 2 h	8.3726(28)	8.3726(28)	2.35	1.32	0.79
800°C 2 h	8.3729(30)	8.3729(30)	3.23	1.70	0.71
700°C 6 h	8.3718(32)	8.3718(32)	6.25	4.73	1.40
800°C 6 h	8.3684(56)	8.3684(56)	6.77	5.15	5.52

be ascribed to defects such as oxygen vacancies and lattice disorders (Malevu & Ocaya, 2015; Vlazan & Stoia, 2018).

The FTIR spectra (Figure 3) confirmed the formation of the $CoFe_2O_4$ nanoparticles via the chemical structure and ion positions. In general, the bands for the metal–oxygen (M–O) interactions in the octahedral sites were located at between 380 and 450 cm^{-1}, whereas those in the tetrahedral sites were typically around 540 and 600 cm^{-1} (Mahhouti *et al*., 2019). The Co-O vibration is indicated by the peak located at 555 cm^{-1}, while the absorption band at 412 cm^{-1} is typically correlated to the Fe–O stretching (Li *et al*., 2023).

No other prominent peaks were observed because the samples were thoroughly dried and exhibited no potential for water absorption on the surfaces during the FTIR measurement, which was consistent with the results of a prior investigation (To Loan *et al*., 2019). The $CoFe_2O_4$ formation was further confirmed

by the Raman spectroscopy measurement (Figure 4). Spinel ferrites exhibited an A_{1g} symmetry that was between 600 and 650 cm^{-1} (Wang *et al*., 2003). The peak at 623 cm^{-1} was assigned to the Fe (Co)–O symmetric stretching (Chandramohan *et al*., 2011; Bartůněk *et al*., 2018). The asymmetric bending of Fe (Co)–O was identified by the band at 470 cm^{-1} (Ojha & Kant, 2021).

The elemental composition of $CoFe_2O_4$ was elucidated by XPS (Figure 5). The Co 2p spectra were deconvoluted [Figure 5 (a)], revealing two

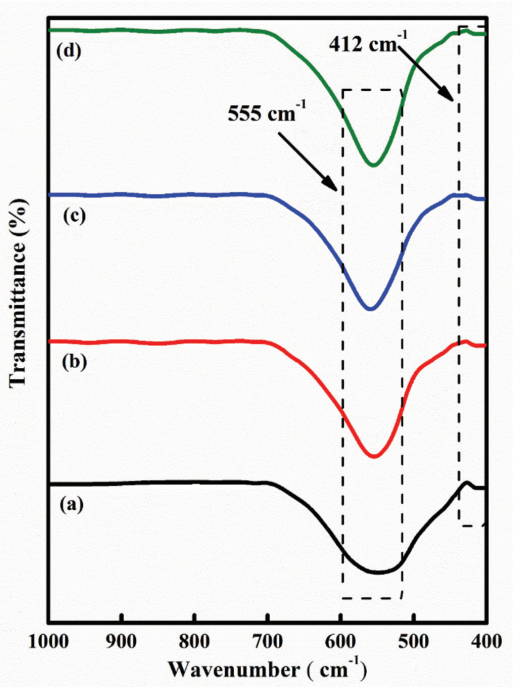

Figure 3: FTIR spectra of samples (a) 700°C 2 h, (b) 800°C 2 h, (c) 700°C 6 h, and (c) 800°C 6 h

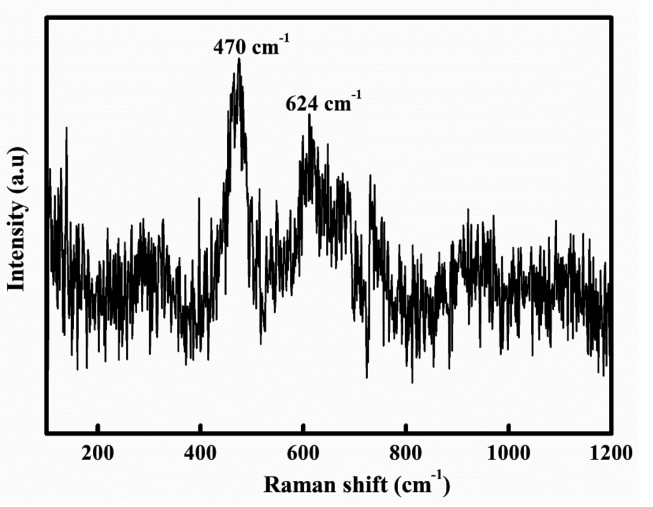

Figure 4: Raman spectroscopy for sample 700°C 2 h

characteristics with binding energies of 778.43 and 794.11 eV, which corresponded to Co $2p_{3/2}$ and Co $2p_{1/2}$, respectively (Wang *et al*., 2021). The two oscillating satellites were also assigned peaks at 783.17 and 801.48 eV (Ahamad *et al*., 2020; Hou *et al*., 2022).

For the Fe 2p spectrum, the presence of Fe^{3+} (709.44 eV) and Fe^{2+} (722.65 eV) was observed in Fe $2p_{3/2}$ and Fe $2p_{1/2}$, respectively [Figure 5 (b)] (Guo *et al*., 2020). Moreover, a broad peak of the O 1s spectrum deconvoluted into three distinct peaks at 527.18, 529.12, and 530.53 eV [Figure 5 (c)] representing the M–O bond and ascribed to the oxygen defects (Sun *et al*., 2017; Wang *et al*., 2021).

Figure 6 presents the SEM images of all samples along with the histogram of the average particle size measured by using ImageJ software. The particles displayed a predominantly spherical shape. For sample 700°C 2 h [Figure 6 (a)], the particles exhibited a uniform spherical size distribution with an average of approximately 0.08 µm, as shown in the corresponding histogram [Figure 6 (b)].

However, when the calcination temperature was raised to 800°C [Figure 6 (a)], the uniformity deteriorated, leading to structural agglomeration and the formation of irregular particles. Despite this, spherical structures remained visible, and the particle size slightly increased to 0.13 µm. The prolonged calcination time to 6 hours in samples 700°C 6 h [Figure 6 (e)] and 800°C 6 h [Figure 6 (g)] led to large particle sizes and the formation of aggregated nanoparticles. The mean particle size also increased from 0.25 to 0.47 µm, as depicted in the size distribution

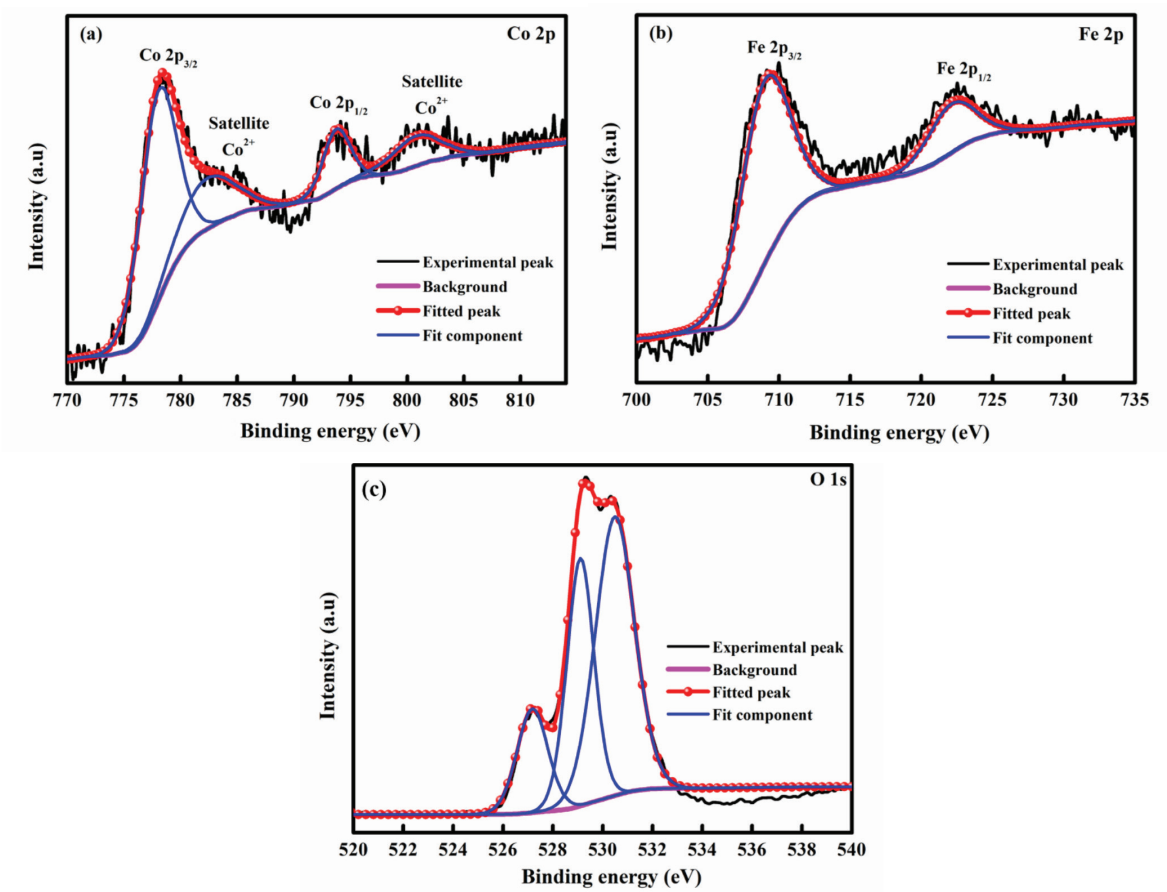

Figure 5: XPS spectroscopy for sample 700°C 2 h

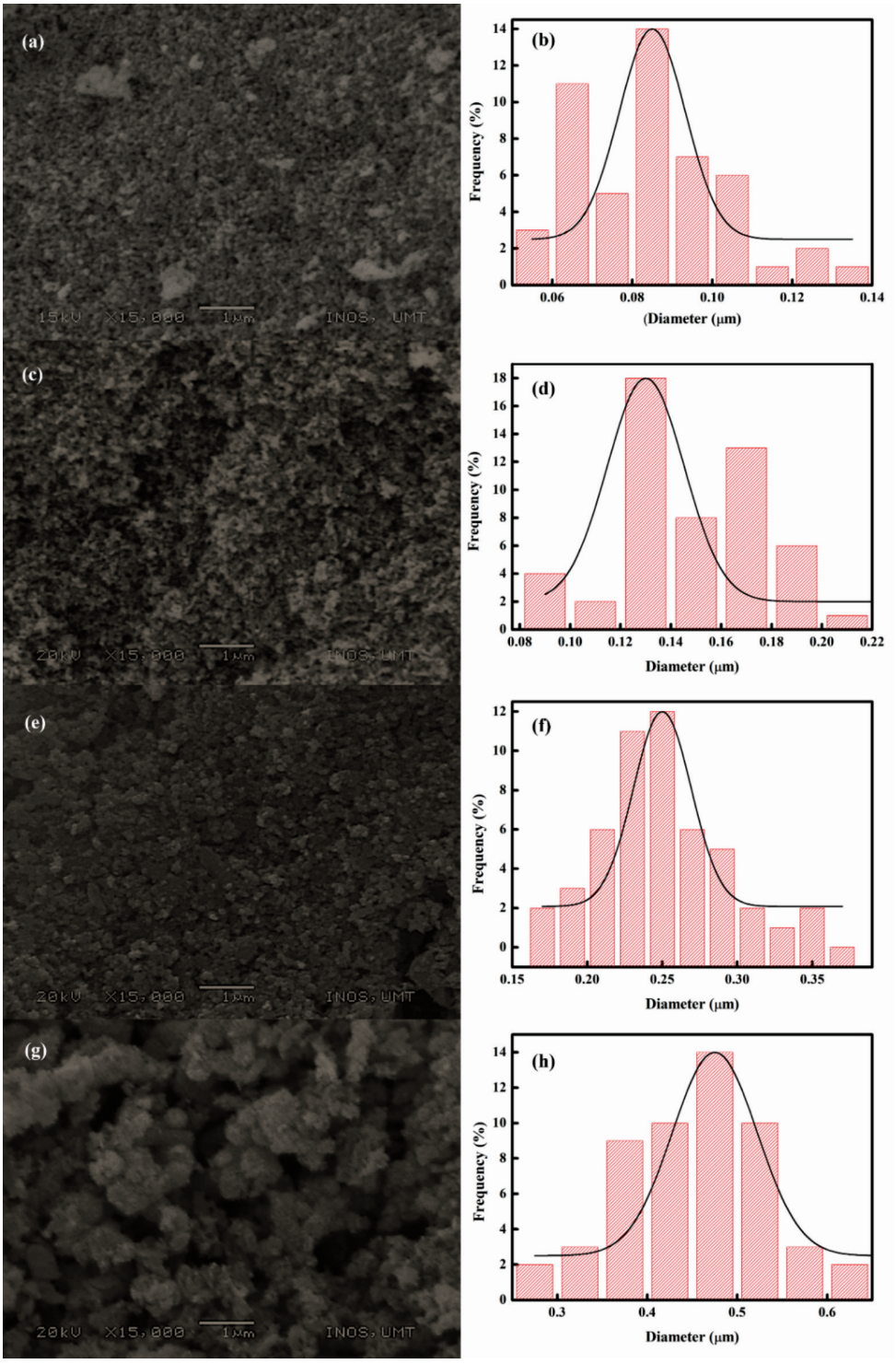

Figure 6: SEM image of $CoFe_2O_4$ and histogram of the particle size distribution (a, b) 700°C 2 h, (c, d) 800°C 2 h, (e, f) 700°C 6 h, and (g, h) 800°C 6 h

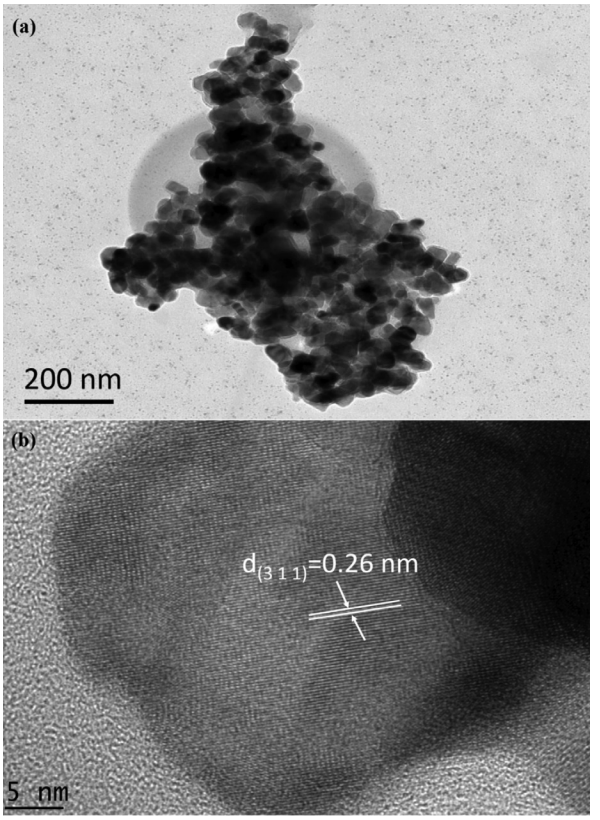

Figure 7: TEM images of sample 700°C 2 h at (a) low magnification and (b) high-resolution TEM image

histograms [Figures 6 (f) and (h)]. At 800°C [Figure 6 (d)], the particles were noticeably bigger and exhibited the maximum degree of agglomeration.

The trend of increasing agglomeration with high calcination temperatures was attributed to the van der Waals forces and the magnetic interactions among the particles (Thimmiah & Nallathambi, 2020). Additionally, these observations were consistent with the XRD results, which showed increased crystallinity correlated with the SEM findings. The smaller crystallite size for sample 700°C 2 h was favourable for producing $CoFe_2O_4$ nanoparticles with smaller particle sizes, resulting in increased surface area and active sites.

As reported in previous studies, smaller particles can enhance the surface area, reduce the diffusion length of Na^+ ions within the particles, and increase the kinetic rates (Yu *et al*., 2016; Fang *et al*., 2019). Furthermore, the TEM images for the sample 700°C 2 h [Figure 7 (a)] confirmed the formation of spherical shapes and the dense agglomeration of crystalline $CoFe_2O_4$, which aligned well with the SEM results. The high-resolution TEM image [Figure 7 (b)] revealed an interplanar spacing of 0.26 nm, which corresponded to the (311) plane of $CoFe_2O_4$.

Figure 8 presents the adsorption–desorption isotherms for the $CoFe_2O_4$ nanoparticle samples. According to the isotherm plots, all samples exhibited type IV adsorption isotherms, as classified by International Union of Pure and Applied Chemistry (IUPAC), indicative of mesoporous structures. Furthermore, all samples exhibited an H3 hysteresis loop exhibiting slit-shaped features caused by slow adsorption at

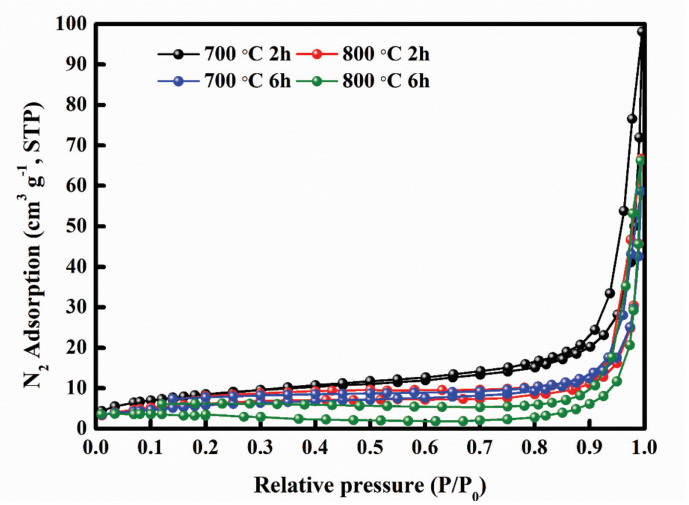

Figure 8: N_2 adsorption–desorption isotherms of $CoFe_2O_4$ nanoparticles

narrow pores (Rahman *et al*., 2021; Idris *et al*., 2023). Table 2 provides the Brunauer–Emmett–Teller (BET) surface area (S_{BET}), pore size, and pore volume of the $CoFe_2O_4$ nanoparticles measured through N_2 gas adsorption.

The results indicated that the highest surface area is achieved when calcined at 700°C for 2 hours, while the lowest surface area was observed at 800°C for 6 hours. The reduction in the surface area and pore volume at 800°C for 6 hours was caused by the agglomerated $CoFe_2O_4$ nanoparticles, crystallite growth, and inter-crystallite sintering; it aligned with literature findings (Shohel *et al*., 2016).

The $CoFe_2O_4$ nanoparticles with a large surface area are advantageous because they reduce the diffusion routes for the charge carriers at the electrode–electrolyte interface, enhance the mass transportation of Na^+ ions, and consequently lower the internal resistance, leading to an improved rate capability (Hou *et al*., 2017). Additionally, the nanoparticles produced under these conditions promoted rapid Na^+ ion migration, resulting in a superior high-rate performance of the batteries.

The electrochemical reactivity of the $CoFe_2O_4$ nanoparticles for sodium storage was evaluated by the cyclic voltammetry (CV) measurement. Figure 9 presents the CV curves of the $CoFe_2O_4$ electrode for the first to fifth cycles. During the first cycle, the primary cathodic peaks at 0.4 and 0.6 V were attributed to the reduction of Fe^{3+} and Co^{2+} to Fe^0 and Co^0, respectively, and the reversible reaction to form Na_2O (Wang *et al*., 2012). In the subsequent cycles, the prominent cathodic peak at 0.6 V upshifted to 0.7 V likely because of the electrode material polarisation (Xing *et al*., 2013). The broad anodic peaks at 0.9 and 2.7 V were most likely associated with the multistep oxidation of

Table 2: BET specific surface area, pore size, and pore volume for all samples

Sample	BET Specific Surface Area, S_{BET} (m^2/g)	Pore Size (nm)	Pore Volume (cm^3/g)
700°C 2 h	31.63	12.2	0.060367
800°C 2 h	22.50	8.0	0.038837
700°C 6 h	21.93	7.0	0.038476
800°C 6 h	10.46	6.7	0.032009

metallic Fe and Co into their respective oxide states (Liu *et al*., 2014; Zhang *et al*., 2015). This result indicated the excellent electrochemical reversibility of the $CoFe_2O_4$ nanosphere electrode. The electrochemical process of $CoFe_2O_4$ in Na-ion batteries is expressed as follows (Zhao *et al*., 2019):

$$CoFe_2O_4 + 8Na^+ + 8e^- \rightarrow Co + 2Fe + 4Na_2O \quad (3)$$

$$4Na_2O + 2Fe + Co \leftrightarrow Fe_2O_3 + CoO + 8Na^+ + 8e^- \quad (4)$$

The selected charge–discharge curves for each electrode at 0.1 A g^{-1} are illustrated in Figure 10. During the first cycle, a solid electrolyte interface layer formed and the electrolyte deteriorated, resulting in an irreversible capacity loss for all electrodes (Chen *et al*., 2016; Zhou *et al*., 2016). However, no apparent plateau was observed in the charge–discharge profiles due to the weak oxidation and reduction peaks in the CV curves, which were consistent with previous research (Zhang *et al*., 2017).

On the basis of these results, the 700°C 2 h electrode delivered a high discharge capacity caused by its homogeneous distribution and small particle sizes, indicating more active sites and a better interfacial contact between the electrode and the electrolytes (Zhou *et al*., 2019). Low discharge capacities for sample 800°C 2 h, 700°C 6 h, and 800°C 6 h electrodes (compared with the 700°C 2 h electrode) were observed because of an unstable reaction between $CoFe_2O_4$ as an active material and the electrolyte, which was caused by the large particle size (Aricò *et al*., 2005). These findings agreed with those of a previous report (Lin *et al*., 2014; Rosedhi *et al*., 2016; Mokhtar *et al*., 2018).

To explore the potential application of the $CoFe_2O_4$ nanoparticles as anode materials for Na-ion batteries, a cycling stability and

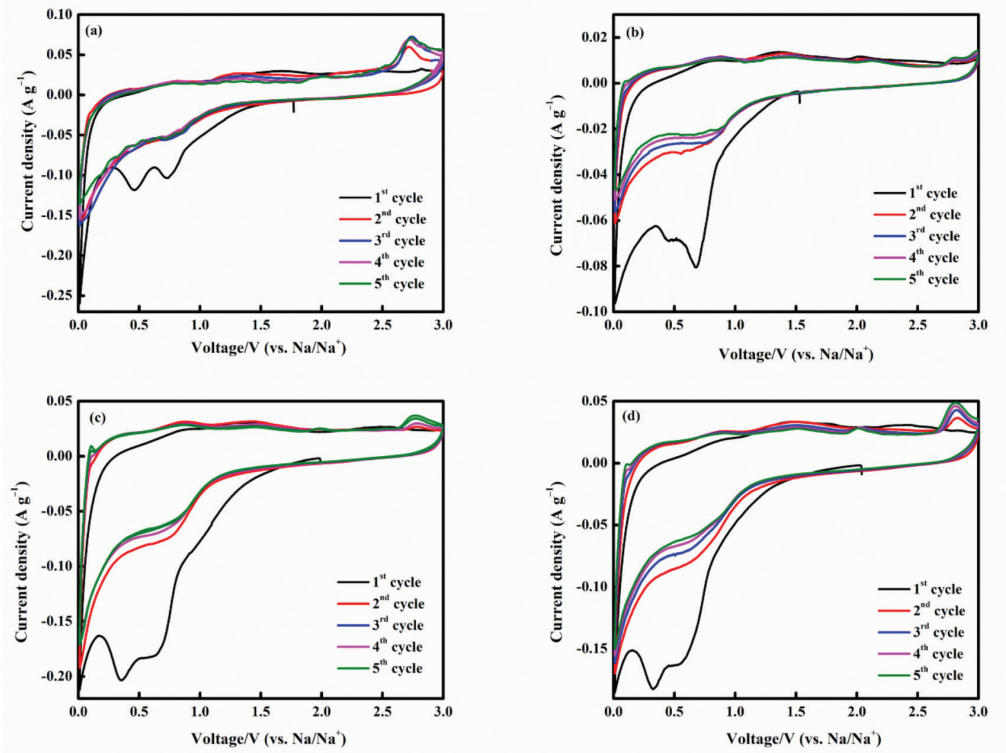

Figure 9: CV measurements of (a) 700°C 2 h, (b) 800°C 2 h, (c) 700°C 6 h, and (d) 800°C 6 h at a scan rate of 0.1 mV s^{-1} (vs. Na/Na^+)

rate capability test was performed (Figure 11). The additional capacity observed during the first discharge was attributed to the formation of the solid electrolyte interface layer, which was consistent with the CV data. During the first cycle, sample 700°C 2 h demonstrated the highest irreversible discharge capacity (1,247 mAh g^{-1}), followed by 800°C 2 h (555 mAh g^{-1}), 700°C 6 h (430 mAh g^{-1}), and 800°C 6 h (187 mAh g^{-1}) electrodes at 0.1 C rate [Figure 11 (a)].

In the second cycle, the discharge capacity of 700°C 2 h electrode remained the highest with 352 mAh g^{-1} and still delivered a discharge capacity of 97 mAh g^{-1} after 100 cycles. Similar patterns were seen for the 800°C 2 h, 700°C 6 h, and 800°C 6 h electrodes. After the second cycle, the 800°C 2 h electrode exhibited a discharge capacity of 154 mAh g^{-1}, gradually decreasing to 76 mAh g^{-1} by the 100th cycle. For the 700°C 6 h and 800°C 6 h electrodes, the discharge capacities were 151 and 86 mAh g^{-1}, respectively, which decreased to 50 and 45 mAh g^{-1} after 100 cycles.

Notably, all electrodes reached a Coulombic efficiency of ~99% after 100 cycles, indicating the formation of stable solid electrolyte interface layers and a high reversibility of the sodiation–desodiation processes around the 100th cycle (Zhang *et al*., 2015; Yu *et al*., 2018). Figure 11 (b) shows the rate capability measurements of all electrodes at the selected current rates. The 700°C 2 h electrode delivered discharge capacities of 189, 103, 70, 55, and 79 mAh g^{-1} at 0.2, 0.4, 0.6, 0.8, and 1.0 C rates, respectively. Even when the current rate was returned to 0.2 C, the reversible capacity remained high, demonstrating a steady cyclability.

In comparison, the discharge capacities of the 800°C 2 h, 700°C 6 h, and 800°C 6 h electrodes were slightly lower at various current densities. These results highlighted that the 700°C 2 h electrode not only demonstrated

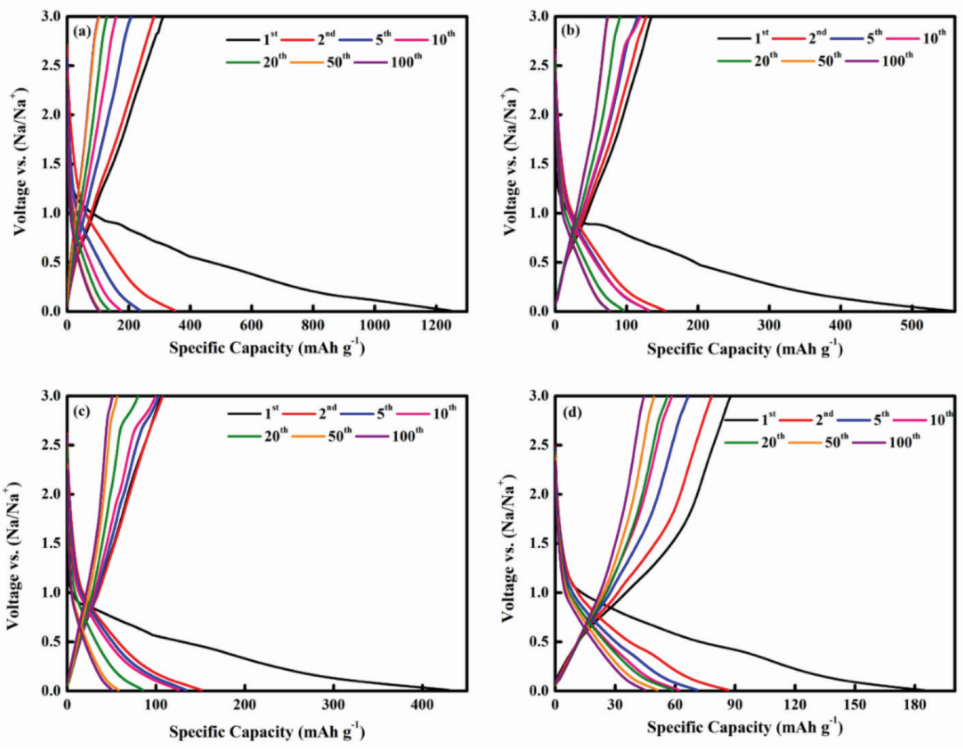

Figure 10: Galvanostatic charge–discharge profiles of (a) 700°C 2 h, (b) 800°C 2 h, (c) 700°C 6 h, and (d) 800°C 6 h electrodes at 0.1 C

acceptable cyclability, but also delivered better rate capability, outperforming the other electrodes. This superior performance was likely attributable to the smaller particle size, which resulted in a larger surface area, more active sites, and improved electrolyte diffusion, leading to a significant increase in the capacitive output (Yu *et al*., 2016; Fang *et al*., 2019).

Based on the results, different calcination temperatures seemed to affect the crystallinity, homogeneity and morphology of the samples, which are the key factors to improving the cycling behaviour of $CoFe_2O_4$ for sodium storage. It is noteworthy that the $CoFe_2O_4$ produced in this work offers several benefits, including small particle sizes, no impurities, and high crystallinity. The acceptable electrochemical performances of $CoFe_2O_4$ may be attributed to the nanosized particles with a high porous structure, which can effectively relieve the stress caused by massive volume changes during the conversion reaction process, thereby enhancing the electrode's structural stability. Specifically, the use of $CoFe_2O_4$ nanoparticles not only addresses the problem of low conductivity but also decreases the distance of diffusivity and increases the rate of Na^+ ion diffusivity.

It is important to highlight that the use of the solvothermal technique is advantageous when preparing $CoFe_2O_4$ nanoparticles. The solvothermal synthesis has emerged as an efficient and controllable method for the preparation of nanosized and crystalline metal oxides (Chang *et al*., 2017; Fu *et al*., 2017; Huang *et al*., 2018; Muruganantham *et al*., 2020).

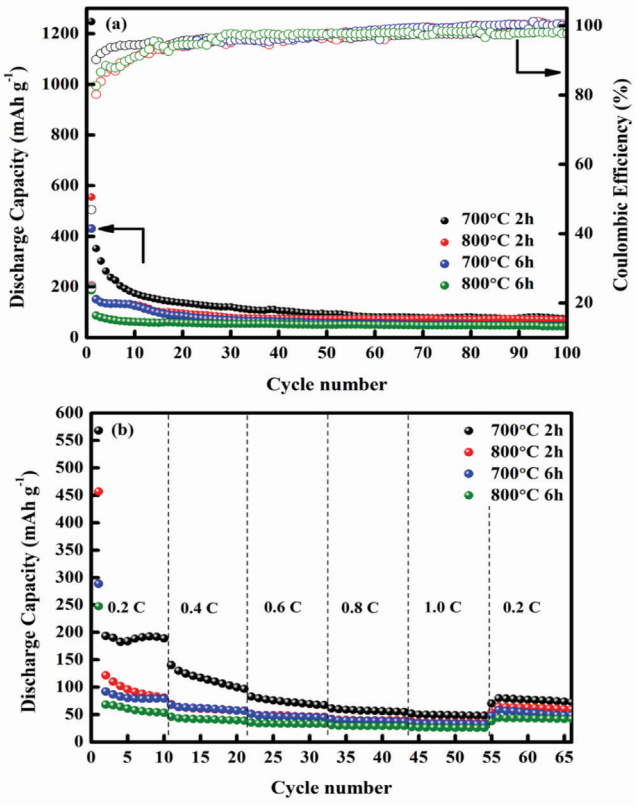

Figure 11: Electrochemical performances of $CoFe_2O_4$ electrodes; (a) cycling performance and corresponding Coulombic efficiency up to 100 cycles at 0.1 C and (b) rate capability at current densities of 0.2, 0.4, 0.6, 0.8, and 1.0 C

Using a sealed autoclave, metathesis reactions can be conducted at low temperatures by heating reactants in a solvent medium. This is achieved by the solvent absorbing the heat generated by the exothermic reactions (Fitch *et al*., 2020). The $CoFe_2O_4$ synthesis at low temperatures utilising the solvothermal process is an efficient, cost-effective, and easy approach for large-scale manufacturing that does not require templates or surfactant. The study findings offer new insights for further investigation on $CoFe_2O_4$ as a potential anode material for Na-ion batteries. Nonetheless, additional investigation is required to enhance the cycling stability and capacity of $CoFe_2O_4$, and reducing the particle size alone might not be enough to completely solve the electrochemical performance issues.

An exploration of surfactant-assisted solvothermal may be worthwhile by altering the droplet size, which can be achieved by manipulating the molar ratio between the surfactant and H_2O (Li *et al*., 2017). Also, combining $CoFe_2O_4$ nanosized particles with a conducting carbon matrix may avoid nanoparticle agglomeration, preserve the conductive contact between particles, and facilitate volume expansion during cycling.

Conclusions

In summary, $CoFe_2O_4$ nanoparticles were synthesised in this work by using the solvothermal method, followed by calcination at 700°C and 800°C for 2 and 6 hours, respectively. The structural analysis confirmed the $CoFe_2O_4$ formation without any impurity. $CoFe_2O_4$ calcined at 700°C for 2 hours exhibited the highest electrochemical activity. At the second cycle and at 0.1 C rate, the $CoFe_2O_4$ possessed a discharge capacity of 352 mAh g^{-1} and reached 102 mAh g^{-1} after 100 cycles.

The electrode also demonstrated a satisfactory rate capability. The smaller particle size and the uniform distribution of the $CoFe_2O_4$ nanoparticles were responsible for enhancing the electrochemical performance by providing large active sites, decreasing the distance of diffusivity, and increasing the rate of Na^+-ion diffusivity, thereby resulting in a better cyclability of the batteries.

Acknowledgements

The project was funded by the Universiti Malaysia Terengganu, through the Research Intensified Grant Scheme (RIGS; Vot 55439). Sarah Umeera Muhamad gratefully acknowledges Yayasan Terengganu for the student scholarships.

Conflict of Interest Statement

The authors declare that they have no conflict of interest.

References

Ahamad, T., Naushad, M., Ubaidullah, M., & Alshehri, S. (2020). Fabrication of highly porous polymeric nanocomposite for the removal of radioactive U(VI) and Eu(III) ions from aqueous solution. *Polymers*, *12*(12), 2940-2955.

Aricò, A. S., Bruce, P., Scrosati, B., Tarascon, J.-M., & van Schalkwijk, W. (2005). Nanostructured materials for advanced energy conversion and storage devices. *Nature Materials*, *4*(5), 366-377.

Bartůněk, V., Sedmidubský, D., Huber, Š., Švecová, M., Ulbrich, P., & Jankovský, O. (2018). Synthesis and properties of nanosized stoichiometric cobalt ferrite spinel. *Materials*, *11*(7), 1241-1252.

Cao, K., Jin, T., Yang, L., & Jiao, L. (2017). Recent progress in conversion reaction metal oxide anodes for Li-ion batteries. *Materials Chemistry Frontiers*, *1*(11), 2213-2242.

Cao, Y., Xiao, L., Sushko, M. L., Wang, W., Schwenzer, B., Xiao, J., Nie, Z., Saraf, L. V., Yang, Z., & Liu, J. (2012). Sodium ion insertion in hollow carbon nanowires for

battery applications. *Nano Letters*, *12*(7), 3783-3787.

Chandramohan, P., Srinivasan, M. P., Velmurugan, S., & Narasimhan, S. V. (2011). Cation distribution and particle size effect on Raman spectrum of $CoFe_2O_4$. *Journal of Solid State Chemistry*, *184*(1), 89-96.

Chang, L., Wang, K., Huang, L., He, Z., Shao, H., & Wang, J. (2017). Hierarchically porous $CoNiO_2$ nanosheet array films with superior sodium storage performance. *New Journal of Chemistry*, *41*(23), 14072-14075.

Chen, J., Ru, Q., Mo, Y., Hu, S., & Hou, X. (2016). Design and synthesis of hollow $NiCo_2O_4$ nanoboxes as anodes for lithium-ion and sodium-ion batteries. *Physical Chemistry Chemical Physics*, *18*(28), 18949-18957.

Dehghanpour, H. R. (2016). $CoFe_2O_4$ nanoparticles structural and magnetic stability relative to ball milling. *Russian Journal of Applied Chemistry*, *89*(5), 846-849.

Ding, J., McCormick, P. G., & Street, R. (1995). Magnetic properties of mechanically alloyed $CoFe_2O_4$. *Solid State Communications*, *95*(1), 31-33.

Duong, H. D. T., Nguyen, D. T., & Kim, K.-S. (2021). Effects of process variables on properties of $CoFe_2O_4$ nanoparticles prepared by solvothermal process. *Nanomaterials*, *11*(11), 3056-3072.

Fang, Y., Yu, X.-Y., & Lou, X. W. (2019). Nanostructured electrode materials for advanced sodium-ion batteries. *Matter*, *1*(1), 90-114.

Feng, J. M., Zhong, X. H., Wang, G. Z., Dong, L., Li, X. F., & Li, D. J. (2017). Hybrid materials of graphene anchored with $CoFe_2O_4$ for the anode in sodium-ion batteries. *Journal of Materials Science*, *52*(6), 3124-3132.

Fitch, S. D. S., Cibin, G., Hepplestone, S. P., Garcia-Araez, N., & Hector, A. L. (2020). Solvothermal synthesis of Sn_3N_4 as a high capacity sodium-ion anode: Theoretical and experimental study of its storage mechanism. *Journal of Materials Chemistry A*, *8*(32), 16437-16450.

Fu, F., Li, J., Yao, Y., Qin, X., Dou, Y., Wang, H., Tsui, J., Chan, K-Y., & Shao, M. (2017). Hierarchical $NiCo_2O_4$ micro- and nanostructures with tunable morphologies as anode materials for lithium- and sodium-ion batteries. *ACS Applied Materials & Interfaces*, *9*(19), 16194-16201.

Gao, R., Yang, Z., Zheng, L., Gu, L., Liu, L., Lee, Y. L., Hu, Z., & Liu, X. (2018). Enhancing the catalytic activity of Co_3O_4 for Li–O_2 batteries through the synergy of surface/interface/doping engineering. *ACS Catalysis*, *8*(3), 1955-1963.

Guo, D., Kang, H., Wei, P., Yang, Y., Hao, Z., Zhang, Q., & Liu, L. (2020). A high-performance bimetallic cobalt iron oxide catalyst for the oxygen evolution reaction. *CrystEngComm*, *22*(25), 4317-4323.

Hariharan, S., Saravanan, K., Ramar, V., & Balaya, P. (2013). A rationally designed dual role anode material for lithium-ion and sodium-ion batteries: Case study of eco-friendly Fe_3O_4. *Physical Chemistry Chemical Physics*, *15*(8), 2945-2953.

He, Q., Rui, K., Chen, C., Yang, J., & Wen, Z. (2017). Interconnected $CoFe_2O_4$–polypyrrole nanotubes as anode materials for high performance sodium ion batteries. *ACS Applied Materials & Interfaces*, *9*(42), 36927-36935.

Hou, H., Shao, L., Zhang, Y., Zou, G., Chen, J., & Ji, X. (2017). Large-area carbon nanosheets doped with phosphorus: A high-performance anode material for sodium-ion batteries. *Advanced Science*, *4*(1), 1600243.

Hou, Z., Liu, C., Gong, J., Wu, J., Sun, S., Zhang, M., & Sun, X. (2022). Micro-structural design of $CoFe_2O_4$/SWCNTs composites

for enhanced electromagnetic properties. *Coatings*, *12*(10), 1532-1546.

Huang, Z.-D., Zhang, T.-T., Lu, H., Masese, T., Yamamoto, K., Liu, R.-Q., Lin, X-J., Feng, X-M., Liu, X-M., Wang, D., Uchimoto, Y., & Ma, Y.-W. (2018). Grain-boundary-rich mesoporous $NiTiO_3$ micro-prism as high tap-density, super rate and long life anode for sodium and lithium ion batteries. *Energy Storage Materials*, *13*, 329-339.

Hwang, J.-Y., Myung, S.-T., & Sun, Y.-K. (2017). Sodium-ion batteries: Present and future. *Chemical Society Reviews*, *46*(12), 3529-3614.

Idris, N. A., Yusoff, H. M., Idris, N. H., Badar, N., Elong, K., Muhamad, S. U., Yusof, N. F. M., & Chia, P. W. (2023). Green synthesis of zinc oxide nanoparticles using leaves extract of mariposa christia vespertilionis and its potential as anode materials in sodium-ion batteries (SIBs). *Arabian Journal for Science and Engineering*, *49*, 623-635.

Jian, Z., Liu, P., Li, F., Chen, M., & Zhou, H. (2014). Monodispersed hierarchical Co_3O_4 spheres intertwined with carbon nanotubes for use as anode materials in sodium-ion batteries. *Journal of Materials Chemistry A*, *2*(34), 13805-13809.

Jiang, Y., Zhang, Z., Liao, H., Zheng, Y., Fu, X., Lu, J., Cheng, S., & Gao, Y. (2024). Progress and prospect of bimetallic oxides for sodium-ion batteries: Synthesis, mechanism, and optimisation strategy. *ACS Nano*, *18*(11), 7796-7824.

Kumar, L., Kumar, P., Narayan, A., & Kar, M. (2013). Rietveld analysis of XRD patterns of different sizes of nanocrystalline cobalt ferrite. *International Nano Letters*, *3*(1), 8-19.

Li, S., Wang, X., Ouyang, F., Liu, R., & Xiong, X. (2023). Novel functional soft magnetic $CoFe_2O_4$/Fe composites: Preparation, characterisation, and low core loss. *Materials*, *16*(10), 3665-3678.

Li, X. H., Xu, C. L., Han, X. H., Qiao, L., Wang, T., & Li, F. S. (2010). Synthesis and magnetic properties of nearly monodisperse $CoFe_2O_4$ nanoparticles through a simple hydrothermal condition. *Nanoscale Research Letters*, *5*(6), 1039-1044.

Li, Y., Wu, X., Wang, S., Wang, W., Xiang, Y., Dai, C., Liu, Z., He, Z., & Wu, X. (2017). Surfactant-assisted solvothermal synthesis of $NiCo_2O_4$ as an anode for lithium-ion batteries. *RSC Advances*, *7*(59), 36909-36916.

Lin, H. B., Zhang, Y. M., Hu, J. N., Wang, Y. T., Xing, L. D., Xu, M. Q., Li, X. P., & Li, W. S. (2014). $LiNi_{0.5}Mn_{1.5}O_4$ nanoparticles: Synthesis with synergistic effect of polyvinylpyrrolidone and ethylene glycol and performance as cathode of lithium ion battery. *Journal of Power Sources*, *257*, 37-44.

Liu, X., Si, W., Zhang, J., Sun, X., Deng, J., Baunack, S., Oswald, S., Liu, L., Yan, C., & Schmidt, O. G. (2014). Free-standing Fe_2O_3 nanomembranes enabling ultra-long cycling life and high rate capability for Li-ion batteries. *Scientific Reports*, *4*(1), 7452.

Mahhouti, Z., El Moussaoui, H., Mahfoud, T., Hamedoun, M., El Marssi, M., Lahmar, A., El Kenz, A., & Benyoussef, A. (2019). Chemical synthesis and magnetic properties of monodisperse cobalt ferrite nanoparticles. *Journal of Materials Science: Materials in Electronics*, *30*(16), 14913-14922.

Malevu, T. D., & Ocaya, R. O. (2015). Effect of annealing temperature on structural, morphology and optical properties of ZnO nano-needles prepared by zinc-air cell system method. *International Journal of Electrochemical Science*, *10*(2), 1752-1761.

Mokhtar, N., Idris, N. H., & Din, M. F. M. (2018). Molten salt synthesis of disordered spinel $LiNi_{0.5}Mn_{1.5}O_4$ with improved electrochemical performance for Li-ion batteries. *International Journal of Electrochemical Science*, *13*(11), 10113-10126.

Muhamad, S. U., Idris, N. H., Yusoff, H. M., Md Din, M. F., Majid, S. R., & Noerochim, L. (2023). Molten salt synthesis of disordered spinel $CoFe_2O_4$ with improved electrochemical performance for sodium-ion batteries. *RSC Advances*, *13*(48), 34200-34209.

Muruganantham, R., Maggay, I. V. B., Huang, J.-Y., Lin, Y.-G., Yang, C.-C., & Liu, W.-R. (2020). Tailoring the mesoporous $ZnMn_2O_4$ spheres as anode materials with excellent cycle stability for sodium-ion batteries. *Journal of Alloys and Compounds*, *844*, 156018-156027.

Ojha, V. H., & Kant, K. M. (2021). Investigation of structural and magnetic properties of strained $CoFe_2O_4$ nanoparticles. *Journal of Physics and Chemistry of Solids*, *148*, 109655-109664.

Prabhakaran, T., Mangalaraja, R. V., Denardin, J. C., & Jiménez, J. A. (2017). The effect of calcination temperature on the structural and magnetic properties of co-precipitated $CoFe_2O_4$ nanoparticles. *Journal of Alloys and Compounds*, *716*, 171-183.

Rafienia, M., Bigham, A., & Hassanzadeh-Tabrizi, S. A. (2018). Solvothermal synthesis of magnetic spinel ferrites. *Journal of Medical Signals & Sensors*, *8*(2), 108-118.

Rahman, M. M., Shafiullah, A. Z., Pal, A., Islam, M. A., Jahan, I., & Saha, B. B. (2021). Study on optimum IUPAC adsorption isotherm models employing sensitivity of parameters for rigorous adsorption system performance evaluation. *Energies*, *14*(22), 7478-7497.

Ranjith Kumar, E., Jayaprakash, R., & Sanjay, K. (2014). Effect of annealing temperature on structural and magnetic properties of manganese substituted $NiFe_2O_4$ nanoparticles. *Materials Science in Semiconductor Processing*, *17*, 173-177.

Repko, A., Nižňanský, D., & Poltierová-Vejpravová, J. (2011). A study of oleic acid-based hydrothermal preparation of $CoFe_2O_4$ nanoparticles. *Journal of Nanoparticle Research*, *13*(10), 5021-5031.

Rosedhi, N. D., Idris, N. H., Rahman, M. M., Din, M. F. M., & Wang, J. (2016). Disordered spinel $LiNi_{0.5}Mn_{1.5}O_4$ cathode with improved rate performance for lithium-ion batteries. *Electrochimica Acta*, *206*, 374-380.

Safi, R., Ghasemi, A., Shoja Razavi, R., Ghasemi, E., & Sodaee, T. (2016). Rietveld structure refinement, cations distribution and magnetic features of $CoFe_2O_4$ nanoparticles synthesized by co-precipitation, hydrothermal, and combustion methods. *Ceramics International*, *42*(5), 6375-6382.

Scrosati, B., Hassoun, J., & Sun, Y.-K. (2011). Lithium-ion batteries. A look into the future. *Energy & Environmental Science*, *4*(9), 3287-3295.

Shohel, M., Miran, M. S., Susan, M. A. B. H., & Mollah, M. Y. A. (2016). Calcination temperature-dependent morphology of photocatalytic ZnO nanoparticles prepared by an electrochemical–thermal method. *Research on Chemical Intermediates*, *42*, 5281-5297.

Sun, X., Zhu, X., Yang, X., Sun, J., Xia, Y., & Yang, D. (2017). $CoFe_2O_4$/carbon nanotube aerogels as high performance anodes for lithium ion batteries. *Green Energy & Environment*, *2*(2), 160-167.

Thimmiah, B. R., & Nallathambi, G. (2020). Synthesis of α-FeO nanoparticles and analyzing the effect of annealing temperature on its properties. *Materials Science-Poland*, *38*(1), 116-121.

To Loan, N. T., Hien Lan, N. T., Thuy Hang, N. T., Quang Hai, N., Tu Anh, D. T., Thi Hau, V., Van Tan, L., & Van Tran, T. (2019). $CoFe_2O_4$ nanomaterials: Effect of annealing temperature on characterisation, magnetic, photocatalytic, and photo-fenton properties. *Processes*, *7*(12), 885-898.

Valvo, M., Lindgren, F., Lafont, U., Björefors, F., & Edström, K. (2014). Towards more

sustainable negative electrodes in Na-ion batteries via nanostructured iron oxide. *Journal of Power Sources*, *245*, 967-978.

Vlazan, P., & Stoia, M. (2018). Structural and magnetic properties of $CoFe_2O_4$ nanopowders, prepared using a modified pechini method. *Ceramics International*, *44*(1), 530-536.

Wang, C., Wang, B., Cao, X., Zhao, J., Chen, L., Shan, L., Wang, H., & Wu, G. (2021). 3D flower-like Co-based oxide composites with excellent wideband electromagnetic microwave absorption. *Composites Part B: Engineering*, *205*, 108529-108538.

Wang, W., Li, W., Wang, S., Miao, Z., Liu, H. K., & Chou, S. (2018). Structural design of anode materials for sodium-ion batteries. *Journal of Materials Chemistry A*, *6*(15), 6183-6205.

Wang, Y., Su, D., Ung, A., Ahn, J.-h., & Wang, G. (2012). Hollow $CoFe_2O_4$ nanospheres as a high capacity anode material for lithium ion batteries. *Nanotechnology*, *23*(5), 055402.

Wang, Z., Schiferl, D., Zhao, Y., & O'Neill, H. S. C. (2003). High pressure raman spectroscopy of spinel-type ferrite $ZnFe_2O_4$. *Journal of Physics and Chemistry of Solids*, *64*(12), 2517-2523.

Xing, Z., Ju, Z., Yang, J., Xu, H., & Qian, Y. (2013). One-step solid state reaction to selectively fabricate cubic and tetragonal $CuFe_2O_4$ anode material for high power lithium ion batteries. *Electrochimica Acta*, *102*, 51-57.

Yan, X., Chen, Z., Wang, Y., Li, H., & Zhang, J. (2018). In-situ growth of ZnO nanoplates on graphene for the application of high rate flexible quasi-solid-state Ni-Zn secondary battery. *Journal of Power Sources*, *407*, 137-146.

Yu, S., Liu, Z., Tempel, H., Kungl, H., & Eichel, R.-A. (2018). Self-standing NASICON-type electrodes with high mass loading for fast-cycling all-phosphate sodium-ion batteries. *Journal of Materials Chemistry A*, *6*(37), 18304-18317.

Yu, X.-Y., Yu, L., & Lou, X. W. (2016). Metal sulfide hollow nanostructures for electrochemical energy storage. *Advanced Energy Materials*, *6*(3), 1501333-1501346.

Yuan, C., Wu, H. B., Xie, Y., & Lou, X. W. (2014). Mixed transition-metal oxides: Design, synthesis, and energy-related applications. *Angewandte Chemie International Edition*, *53*(6), 1488-1504.

Zhang, X., Li, D., Zhu, G., Lu, T., & Pan, L. (2017). Porous $CoFe_2O_4$ nanocubes derived from metal-organic frameworks as high-performance anode for sodium ion batteries. *Journal of Colloid and Interface Science*, *499*, 145-150.

Zhang, Z., Li, W., Zou, R., Kang, W., San Chui, Y., Yuen, M. F., Lee, C-S., & Zhang, W. (2015). Layer-stacked cobalt ferrite ($CoFe_2O_4$) mesoporous platelets for high-performance lithium ion battery anodes. *Journal of Materials Chemistry A*, *3*(13), 6990-6997.

Zhao, M., Xiong, J., Yang, Y., & Zhao, J. (2019). Template-assisted synthesis of honeycomb-like $CoFe_2O_4$/CNTs/rGO composite as anode material for Li/Na-ion batteries. *ChemElectroChem*, *6*(13), 3468-3477.

Zhou, D., Xue, L. P., & Wang, N. (2019). Three-dimensional porous $CoFe_2O_4$/graphene composite for highly stable sodium-ion batteries. *ChemElectroChem*, *6*(5), 1552-1557.

Zhou, Y., Sun, W., Rui, X., Zhou, Y., Ng, W. J., Yan, Q., & Fong, E. (2016). Biochemistry-derived porous carbon-encapsulated metal oxide nanocrystals for enhanced sodium storage. *Nano Energy*, *21*, 71-79.